materials

MDPI

Article

Viscoelasticity in Large Deformation Analysis of Hyperelastic Structures

Shahriar Dastjerdi [1], Bekir Akgöz [1,*] and Ömer Civalek [1,2]

[1] Division of Mechanics, Civil Engineering Department, Akdeniz University, Antalya 07070, Turkey
[2] Department of Medical Research, China Medical University Hospital, China Medical University, Taichung 404, Taiwan
* Correspondence: bekirakgoz@akdeniz.edu.tr

Abstract: In this paper, an annular/circular plate made of hyperelastic material and considering the viscoelastic property was investigated based on a novel nonlinear elasticity theory. A new approach for hyperelastic materials in conjunction with the Kelvin–Voigt scheme is employed to obtain the structure's large deformation under uniform transverse loading. The constitutive equations were extracted using the energy method. The derived partial differential time-dependent equations have been solved via the semi-analytical polynomial method (SAPM). The obtained results have been validated by ABAQUS software and the available paper. In consequence, a good agreement between the results was observed. Finally, several affecting parameters on the analysis have been attended to and studied, such as the nonlinear elasticity analysis, the boundary conditions, loading, and the material's viscosity. It can be possible to obtain the needed time for achieving the final deformation of the structure based on the applied analysis in this research.

Keywords: nonlinear hyperelastic material; viscoelasticity; semi-analytical polynomial method; large deformation

check for updates

Citation: Dastjerdi, S.; Akgöz, B.; Civalek, Ö. Viscoelasticity in Large Deformation Analysis of Hyperelastic Structures. *Materials* **2022**, *15*, 8425. https://doi.org/10.3390/ma15238425

Academic Editors: Abbas S. Milani, Michele Bacciocchi and Rui Miranda Guedes

Received: 12 October 2022
Accepted: 23 November 2022
Published: 26 November 2022

Publisher's Note: MDPI stays neutral with regard to jurisdictional claims in published maps and institutional affiliations.

Copyright: © 2022 by the authors. Licensee MDPI, Basel, Switzerland. This article is an open access article distributed under the terms and conditions of the Creative Commons Attribution (CC BY) license (https://creativecommons.org/licenses/by/4.0/).

1. Introduction

Various materials can be found in nature that demonstrate different mechanical behaviors under applied loads, such as metals displaying linear elastic behavior until yielding. At the same time, irreversible deformation is then observed up to failure. On the other hand, brittle materials exhibit a slight elastic deformation linearly and then fail without irreversible deformation. However, it is notable that all materials do not exhibit linear elasticity. Hyperelastic materials will exhibit elastic deformations excessively before failure without irreversible deformation. These materials exhibit an extremely nonlinear stress-strain behavior that ascends monotonically up to fracture. It is well-known that linear elastic materials can be defined with two material constants: modulus of elasticity and Poisson's ratio. On the contrary, hyperelastic materials can be defined by a strain-energy density function. The stored strain energy remains constant when a sample is subjected to constant strain. Therefore, hyperelastic materials are modeled in the context of strain energy potentials such as Arruda-Boyce [1], Gent [2], Neo-Hookean [3], and Yeoh [4].

Some recent studies on the mechanical responses of hyperelastic structures are summarized below. Erchiqui et al. [5] implemented a dynamic finite element method to model the visco-hyperelastic behaviors of a thin, isotropic, and incompressible thermoplastic membrane based on the Ogden and Mooney-Rivlin models. Kocatürk and Akbaş [6] examined the geometrically nonlinear static response of a hyperelastic simply supported beam under a non-follower load by the finite element and Newton–Raphson iteration methods. Li et al. [7] perused the dynamic behavior of the visco-hyperelastic dielectric elastomer structures based on the Gent hyperelastic model. Alibakhshi et al. [8] analyzed the nonlinear vibration of dielectric elastomer microbeam resonators based on a hyperelastic Cosserat

model by the Runge-Kutta time domain method. Almasi et al. [9] studied the thermomechanical analysis of a hyperelastic thick cylindrical pressure vessel by giving analytical and numerical solutions. Asgari and Hashemi [10] developed an efficient visco-hyperelastic constitutive model for a hollow cylinder elastomer under dynamic and impact loadings. Pascon [11,12] implemented a finite element formulation based on a two-dimensional beam element to investigate various viscoelastic functionally graded materials and beams made of functionally graded hyperelastic material. The constitutive equations are extracted based on the neo-Hookean model. Gharooni and Ghannad [13] studied the nonlinear analysis of functionally graded tapered hyperelastic cylindrical pressure vessels subjected to non-uniform pressure load.

Hosseini and Rahimi [14] conducted the nonlinear bending analysis of a neo-Hookean hyperelastic plate based on the Mindlin plate theory. Xu et al. [15] introduced the plate element formulation by quadratic interpolation. They carried out static and dynamic analyses of incompressible hyperelastic silicone plates. Dadgar-Rad and Firouzi [16] presented a nonlinear finite element formulation for the viscoelastic deformation of hyperelastic structures under several loadings and boundary conditions. Ansari et al. [17] developed a numerical approach to survey the deformations of hyperelastic Mindlin rectangular plates in compressible and nearly incompressible regimes based on the Neo-Hookean model. Tashiro et al. [18] analyzed blood clots using a nonlinear viscoelastic and hyperelastic model. They employed the visco-hyperelastic finite element method to estimate the mechanical behavior of blood clots. Shariyat and Abadi [19] studied the nonlinear dynamic and impact responses of incompressible neo-Hookean hyperelastic plates with stiff elastic reinforcing particles. Runge-Kutta time integration and penalty methods are used in the solution. Karimi et al. [20] conducted the nonlinear dynamic analysis of an embedded neo-Hookean hyperelastic membrane under a uniformly distributed hydrostatic pressure. Alibakhshi and Heidari [21] carried out the nonlinear vibration of a dielectric elastomer balloon via the Gent hyperelastic model. A time integration-based solver is utilized to solve the resulting equations. Alibakhshi et al. [22] elaborated on a suitable detection mechanism for scanning the surface profile of a micro-sample by AFM, considering that the probe is made of a hyperelastic material. Falope et al. [23] proposed a finite element-based theoretical model to study the bending behavior of a hyperelastic solid.

Hosseini et al. [24] perused the nonlinear static behavior of functionally graded hyperelastic plates based on FSDT. The potential energy function is formulated according to the neo-Hookean model and the Cauchy–Green tensor. Coda et al. [25] elaborated a finite element formulation to analyze the laminated and functionally graded hyperelastic one-dimensional structure with transverse shear stress distribution. Dastjerdi et al. [26] introduced a comprehensive theoretical method to examine the mechanical responses of hyperelastic structures. The proposed method can analyze the geometrically and physically nonlinear hyperelastic materials. Zhao et al. [27] investigated the nonlinear dynamic responses of the visco-hyperelastic spherical shells under uniform radial loads. Additionally, Zhao et al. [28] perused dynamic loads and structural damping influences for incompressible hyperelastic spherical shells. They considered the Yeoh strain energy function in their study. Bacciocchi and Tarantino [29] examined the finite bending of hyperelastic beams based on the compressible Mooney-Rivlin model. More information about the nonlinear dynamics of hyperelastic structures can be found in the recent review article [30]. Additionally, many studies have been carried out on analyzing viscoelastic structures [31–45]. Li et al. [46] presented a perturbation approach for the lateral vibration analysis of viscoelastic microstructures. The clamped microbeam has been subjected to external harmonic excitation. Recently, some researchers developed a structure-preserving approach to solve the macroscopic/microscopic coupling dynamic problems with large deformation [47]. Additionally, a large deformation analysis of a nano-sized structure has been attended by Yan et al. [48].

As stated before, many recent studies have been performed on the mechanical analysis of structures made of hyperelastic materials based on various strain energy functions,

especially the neo-Hookean model. However, there is no study on the static response of an annular circular visco-hyperelastic plate. The new approach for hyperelastic materials simulates the annular circular visco-hyperelastic plate in conjunction with the Kelvin–Voigt scheme. The general formulations are derived according to the first-order shear deformation theory (FSDT). The constitutive equations and boundary conditions are extracted by the energy method. Then, the semi-analytical polynomial method is utilized for solving the partial differential time-dependent equations. Finally, the effects of various parameters on the bending analysis of the annular circular visco-hyperelastic plate are investigated and discussed in detail.

2. Geometry of the Structure

First, the geometry of the problem is discussed. The geometry of the analyzed structure will play a significant role in obtaining the governing equations. The more comprehensive the geometry of the problem, the more different structures can be modeled only by considering a single formulation. Analysis of the structures made of hyperelastic materials will make the simulation more complicated. Therefore, an attempt has been made to focus more on the effect of viscosity on hyperelastic materials. Hence, an annular–circular structure made of visco-hyperelastic material has been assumed. The geometry of the analyzed problem is shown in Figure 1, along with the considered coordinate system, which is the cylindrical coordinate system.

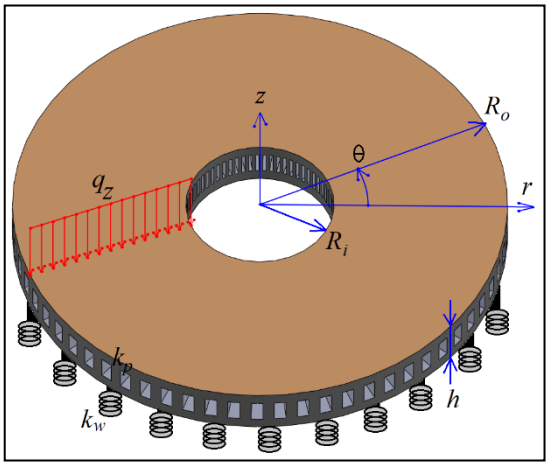


Figure 1. Schematic view of the structure.

As can be seen, the inner radius of the structure is R_i, and its outer radius is R_o. Additionally, the thickness of the structure is constant and equal to h. The structure is placed on an elastic foundation with two components, the Winkler (k_w) and Pasternak (k_p). The external load on the structure is considered a uniform distributed load in the z direction equal to q_z.

3. Viscoelastic Property

In this research, an attempt has been made to perform two nonlinear elastic properties simultaneously with the changes in the deformation of the material with respect to the strain rate. In other words, large strains against the strain rate are considered. The structure's material is considered in such a way that the deformation created in it due to the applied load is different during the duration of the load application. On the other hand, the final deformation of the structure does not happen as soon as the load is applied, and it takes place over time. The Kelvin–Voigt model is used to consider the viscoelastic properties of the material [43]. Additionally, other models such as Zener and mixing linear viscoelasticity and nonlinear elasticity (as has been done in this paper) have been used by other researchers [49,50]. In this type of time-dependent modeling for stress–strain, a spring and a damper are placed in parallel, which can be seen in Figure 2. As shown in

Figure 2, the viscous property of the material (time-dependent strain) is simulated by a damper. Additionally, the material's elasticity is modeled by a spring (E represents Young's elasticity modulus). In linear elastic materials, the value of E is constant and changes linearly. However, this value is not fixed or variable in this research. Therefore, the model (as explained in the next part) uses linear viscoelasticity according to the Kelvin–Voigt scheme. However, the principle of elasticity has been considered nonlinearly.

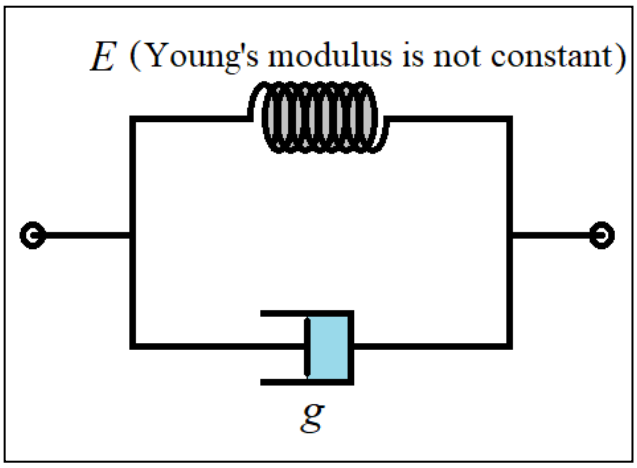


Figure 2. The Kelvin–Voigt model for viscoelastic property.

Stress and strain will be written according to the following equations based on the Kelvin–Voigt simulation.

$$\sigma_{Total} = \sigma_s + \sigma_D \left(\sigma_s = E\varepsilon(r,\theta,z,t), \sigma_D = g\frac{\partial \varepsilon(r,\theta,z,t)}{\partial t} \right) \quad (1)$$

It can be seen in Figure 2 that E is the elasticity modulus, and g is the viscosity of the material. The amount of σ_s is linear here according to Equation (1). However, it is not constant in this study due to the nonlinear elasticity analysis. This issue will be discussed in detail in the next part.

4. Nonlinear Elastic Material and Governing Equations

In a linear elastic material, it can be observed that the changes in stress and strain are linear. However, in a structure with nonlinear elastic property, the stress increases nonlinearly with the increase of strain. In this research, the material with nonlinear elastic properties is assumed. Therefore, calculations based on nonlinear elasticity theory are considered. Various mathematical simulations and theories have been presented regarding the analysis of nonlinear elastic or hyperelastic structures [2,9–12]. A new method has been presented previously for analyzing the mechanical behavior of nonlinear elastic structures [26]. According to this theory, the stress-strain diagram of a nonlinear elastic material obtained from the experiment is approximated by a polynomial function ($\sigma(\varepsilon) = \sum_{i=1}^{n} E_i \varepsilon^i$). According to the polynomial degree, a higher accuracy can be obtained by choosing more n. Consequently, the expressed viscous stress can be formulated as $\sigma_s(\varepsilon) = \sum_{i=1}^{n} E_i \varepsilon(r,\theta,z,t)^i$. The calculations related to the strain field and the governing equations can be obtained according to the following equations by considering the viscoelastic property.

$$\overleftrightarrow{\varepsilon}_{ij} = \begin{bmatrix} \varepsilon_{rr} & \varepsilon_{r\theta} & \varepsilon_{rz} \\ \varepsilon_{\theta r} & \varepsilon_{\theta\theta} & \varepsilon_{\theta z} \\ \varepsilon_{zr} & \varepsilon_{z\theta} & \varepsilon_{zz} \end{bmatrix}$$

$$\begin{aligned}\varepsilon_{rr} = \left(1+g\frac{\partial}{\partial t}\right) & \left(\frac{\partial U_r}{\partial r}+\frac{1}{2}\left(\frac{\partial U_z}{\partial r}\right)^2\right); 2\varepsilon_{r\theta}=2\varepsilon_{\theta r}=0;\ 2\varepsilon_{rz}=2\varepsilon_{zr}\\ &= \left(1+g\frac{\partial}{\partial t}\right)\left(\frac{\partial U_r}{\partial z}+\frac{\partial U_z}{\partial r}\right);\ \varepsilon_{\theta\theta}\\ &= \left(1+g\frac{\partial}{\partial t}\right)\left(\frac{1}{r}\left(\frac{\partial U_\theta}{\partial \theta}+U_r\right)\right);\ 2\varepsilon_{\theta z}=2\varepsilon_{z\theta}=0;\ \varepsilon_{zz}=0\end{aligned} \tag{2}$$

The strain field is assumed based on FSDT as

$$\begin{cases} U_r(r,z,t) = u_0(r,t)+z\varphi(r,t)\\ U_\theta(r,z)=0\\ U_z(r,z,t)=w_0(r,t)\end{cases} \tag{3}$$

$$\sigma_{rr}=\sum_{i=1}^{n}\frac{E_i}{(1-\nu^2)^i}[\varepsilon_{rr}+\nu\varepsilon_{\theta\theta}]^i;\sigma_{\theta\theta}=\sum_{i=1}^{n}\frac{E_i}{(1-\nu^2)^i}[\varepsilon_{\theta\theta}+\nu\varepsilon_{rr}]^i;$$

$$\sigma_{rz}=\sum_{i=1}^{n}\frac{E_i}{[2(1+\nu)]^i}\varepsilon_{rz}^i \tag{4}$$

In the above equations, u_0 and w_0 are transport displacements, and φ is the rotation function around the θ axes. Now, using the energy method [43–45] ($\delta P_{Total}=\iiint_V \sigma_{ij}\delta\varepsilon_{ij}+\iint_A\left(q_z-k_W w_0+k_p\nabla^2 w_0\right)\delta w_0\ (i,j=r,\theta,z)$), the mathematical description of boundary conditions and governing equations can be introduced as the following equations.

$$\delta u_0: \frac{\partial N_{rr}}{\partial r}+\frac{1}{r}(N_{rr}-N_{\theta\theta})=0 \tag{5}$$

$$\delta w_0: \frac{\partial N_{rz}}{\partial r}+\frac{N_{rz}}{r}+N_{rr}\frac{\partial^2 w_0}{\partial r^2}+\frac{N_{rr}}{r}\frac{\partial w_0}{\partial r}+\frac{\partial N_{rr}}{\partial r}\frac{\partial w_0}{\partial r}+q_z-k_w w_0+k_p\nabla^2(w_0)=0 \tag{6}$$

$$\delta\varphi: \frac{\partial M_{rr}}{\partial r}+\frac{1}{r}(M_{rr}-M_{\theta\theta})-N_{rz}=0 \tag{7}$$

$$(N_{rr},N_{\theta\theta},N_{rz})=\int_{-\frac{h}{2}}^{\frac{h}{2}}(\sigma_{rr},\sigma_{\theta\theta},\sigma_{rz})dz;\ (M_{rr},M_{\theta\theta})=\int_{-\frac{h}{2}}^{\frac{h}{2}}(\sigma_{rr},\sigma_{\theta\theta},)zdz \tag{8}$$

Considering the uniform transverse load on the structure, the problem is symmetrical, and there will be no changes in the θ direction. The only independent variables of the problem are r and t, where t represents the time duration. The mathematical definition of the different types of boundary conditions is introduced according to the following relations: Clamped (C), Simply supported (S), and Free (F) at the edges of $r=R_i,\ R_o$.

$$\begin{cases} Clamped:\ u_0=w_0=\varphi=0\ (r=R_i,\ R_o;t=0,t_N)\\ Simply\ supported:\ u_0=w_0=M_{rr}=0\ (r=R_i,\ R_o;t=0,t_N)\\ Free:\ N_{rr}=N_{rz}=M_{rr}=0\ (r=R_i,\ R_o;t=0,t_N)\end{cases} \tag{9}$$

5. Solution Method

This research uses the semi-analytical method based on polynomials (SAPM) to solve the governing equations [43,44]. According to this method, the displacement functions (u_0, w_0, and φ) are formulated as comprehensive polynomials based on the number of nodes (N and M) in each direction of the independent variable of the problem (r and z).

$$u_0(r,z)=\sum_{i=1}^{N}\sum_{j=1}^{M}a_{(j+M(i-1))}r^{(i-1)}t^{(j-1)} \tag{10}$$

$$w_0(r,z)=\sum_{i=1}^{N}\sum_{j=1}^{M}a_{(j+M(i-1)+M\cdot N)}r^{(i-1)}t^{(j-1)} \tag{11}$$

$$\varphi(r,z) = \sum_{i=1}^{N}\sum_{j=1}^{M} a_{(j+M(i-1)+2M\cdot N)} r^{(i-1)} t^{(j-1)} \tag{12}$$

Now, a system of algebraic equations can be obtained by inserting the functions (Equations (10)–(12)) in the mathematical definition of the boundary conditions at the edges and constitutive equations. Finally, by solving the obtained algebraic equations, the unknown functions in the displacement field and, accordingly, other unknowns, including stresses and strains, will be obtained for the visco-hyperelastic annular–circular sheet under uniform transverse load.

6. Discussion

6.1. Validation

6.1.1. The Solving Method (SAPM)

First, the accuracy of the used solution method is checked. Figure 3 shows the background changes in terms of time for an annular/circular sheet with the following specifications for different values of the number of nodes in the direction of r and t.

$$R_i = 0.1m, R_o = 0.5m, h = 0.03m, E_1 = 2.1467 \times 10^6, E_2 = -6.4659 \times 10^5, E_3 = -69779, E_4 = 5.66989 \times 10^5, \nu = 0.3, q_z = 1000Pa, \tag{13}$$

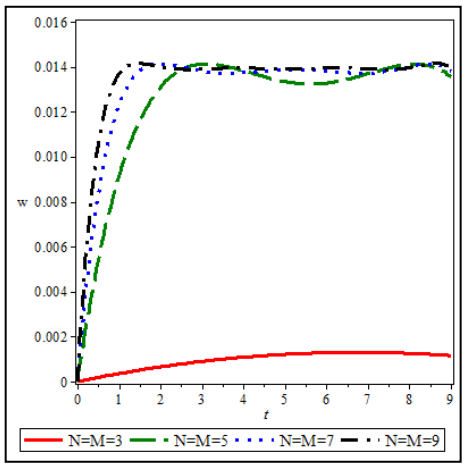


Figure 3. Investigation of the result's convergence.

As can be seen, the accuracy of the results increases versus the increase of nodes in the calculations. A sudden jump is observed between the results of $N = M = 3$ and $N = M = 5$, so the used solution method has a very high convergence. It can be seen that the results of seven and nine nodes are very close, and therefore, the results obtained from seven or nine nodes can be used with reasonable confidence. Increasing the number of nodes in the calculations will significantly increase the time to obtain the results. Therefore, the optimized number of nodes in the network for solving the problem is an important point that should be considered. In the first form, by choosing only nine nodes in each direction (r and t), you can get the results with the desired accuracy for the subsequent analysis.

6.1.2. Comparisons

Figure 4a,b and Table 1 are provided to validate the results. Figure 4 shows the maximum deflection between the results of (a) the present study and (b) the obtained results of ABAQUS software for an annular/circular plate. It is demonstrated that the results agree well. Finding relevant papers in visco-hyperelasticity to fit with the present work is hard. For example, some papers can be found. However, their modeled geometry might be different from the present study. Another assessment was done, and the results can be observed in Figure 5 for the visco-hyperelastic structure. As the tested model [51] is a thick circular sheet, we considered a quasi-three-dimensional analysis [52]. Therefore, the

captured results have been monitored into a single plot in conjunction with the experimental results [51]. The compared results in Figure 5 show that an acceptable difference is available between the obtained results. The obtained results in this paper are near to the ABAQUS results, according to the originally depicted figure in [51]. Eventually, the applied theory and solving method are reliable. Additionally, according to Table 1, the same conclusion can be made for different boundary conditions.

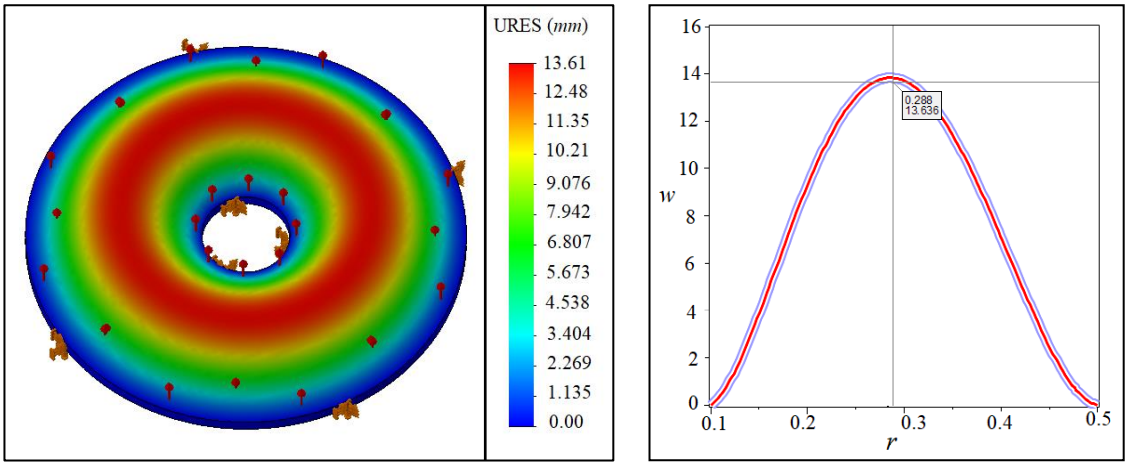


Figure 4. Deflection results of (**a**) ABAQUS software and (**b**) the present study.

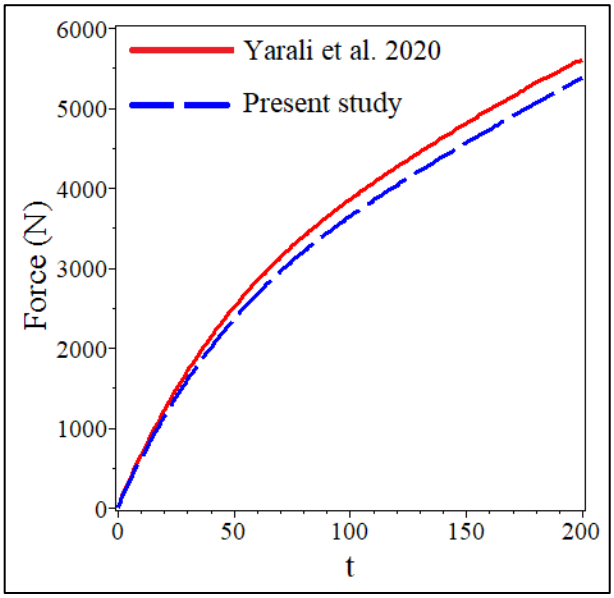


Figure 5. Comparison between the results of this study and [51] for the visco-hyperelastic analysis.

Table 1. Comparison between the maximum deflection (mm) results of the present study and [53] for aluminum circular plates.

Boundary Conditions	Maximum Deflection (mm)							
	$q_z = 5\ MPa$		$q_z = 20\ MPa$		$q_z = 50\ MPa$		$q_z = 100\ MPa$	
	Present	**[53]**	**Present**	**[53]**	**Present**	**[53]**	**Present**	**[53]**
SS	3.789	3.883	8.232	8.333	12.11	12.15	15.56	15.68
CC	1.261	1.263	4.559	4.562	8.819	8.820	12.93	12.93

6.2. Numerical Results

To investigate different boundary conditions on nonlinear-elastic analysis, Figure 6 depicts a circular sheet with the same characteristics as Figure 3. As can be seen, the maximum deflection increases with the increase of transverse load on the structure. The increase in the maximum deflection is completely nonlinear and will be accompanied by a decreasing slope. In other words, as the transverse load on the sheet increases, it is observed that the slope of the changes decreases. The importance of this matter is that if the linear analysis were considered, the obtained results would increase linearly. These linear results would be acceptable only for low load values. However, because the nonlinear analysis of the sheet made of material with nonlinear elastic properties has been studied in this research, the simulation results can be used with appropriate accuracy. Another point (according to Figure 6, which is drawn for two boundary conditions, *CC* and *SS*, at the edges of R_i and R_o) is that the decreasing trend of the results at the beginning of loading is more for the *CC* boundary conditions than SS. However, with increasing load on the plate, the changes are almost the same, with a slight difference for the two boundary conditions, *CC* and *SS*. In other words, by increasing the load on the structure, the effects related to the boundary conditions are reduced, and the behavior of the sheet against the applied load will be less affected by the applied boundary conditions.

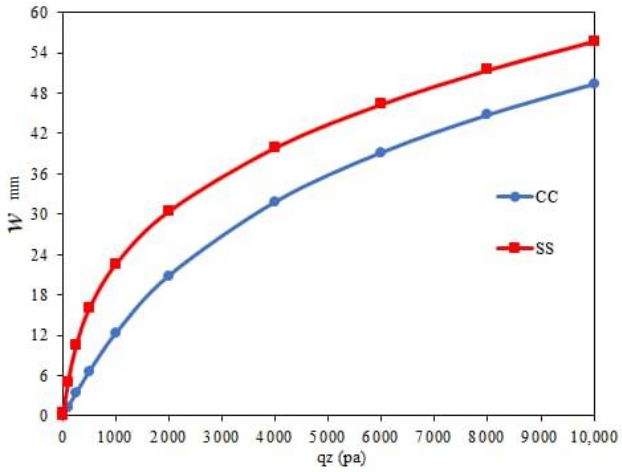


Figure 6. Deflection changes versus the applied transverse loading (q_z) for different types of boundary conditions.

The viscoelastic property in nonlinear elasticity analysis is a significant issue considered in this research. Therefore, Figures 7 and 8 show the effect of viscosity (changes in deformation over time) on the results of the maximum deflection of the circular sheet (specifications of Figure 3). Viscosity $g = 0$ means that, when the load is applied on the sheet, the maximum deflection will occur, and the structure will reach the absolute limit of deformation, which can be seen in Figure 7. Of course, it can be observed that the mentioned result will be for $t = 1s$. This calculation error is due to the limitation in choosing the number of nodes in time when solving the governing equations. It can be observed that with the rise of the viscosity value (g), the needed time for the sheet to reach its final deformation will increase. In other words, with the increase in viscosity, the slope variations will decrease over time. Of course, the effect of viscosity on the results is not linear. In other words, the distance between the results from $g = 0$ to $g = 5$ is more remarkable than from $g = 5$ to $g = 10$. As the viscosity of the structure material increases, the intensity of its impact on the results decreases. Figure 8 is one of the results of the curves in Figure 7 ($g = 5$), which here show the changes in the deflection in two directions: r and t, simultaneously. According to Figure 8, the maximum deflection on the sheet will occur in its middle ($r = R_i,\ R_o$), according to the *CC* boundary conditions.

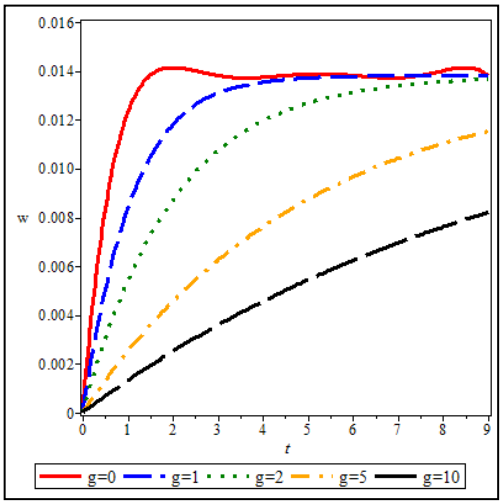


Figure 7. Viscoelastic effects on the results.

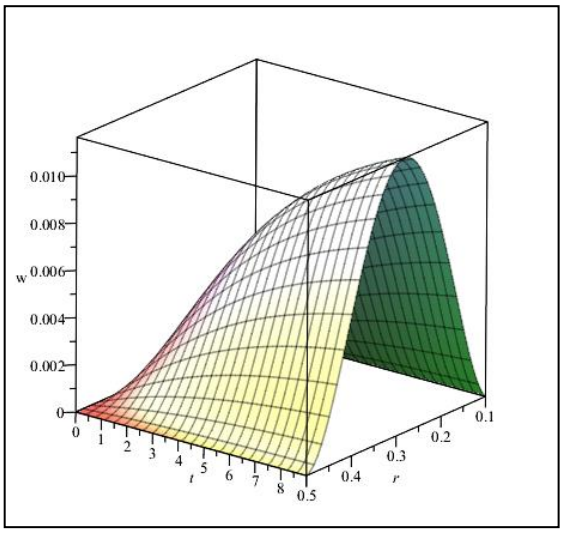


Figure 8. Three-dimensional view of deflection changes versus r and time (t) for $g = 5$.

In Figures 7 and 8, the effect of viscosity on the nonlinear elastic structure is investigated. As seen, with the increase in viscosity, the time for the structure to reach its final shape increases. Now, this topic, how much time is required for the final deflection (considering a specific viscosity), is further investigated. Figure 9a is drawn for viscosity $g = 5$, and Figure 9b is drawn for $g = 10$. Here, the criterion for drawing two shapes is to reach the absolute limit of the deformation and be equal to a specific number. In other words, the final deflection for both Figure 9a,b is equal. It can be seen that the final deflection in Figure 9a is for $t = 25s$. However, this result in Figure 9b is equal to $t = 50s$. This analysis is crucial, because it is observed that, with the doubling of the viscosity of the structure, the time it takes to reach the final shape change also doubles. Although the variation rate is nonlinear, the deformation of the structure at the final time has a linear and direct relationship with the value of the viscosity of the structure. Of course, this conclusion has been reached for this particular problem. Such a result may not be obtained by considering other assumptions, including environmental factors such as temperature, humidity, or electric fields. Investigating the impact of the mentioned factors can also be considered by other researchers who work in this field.

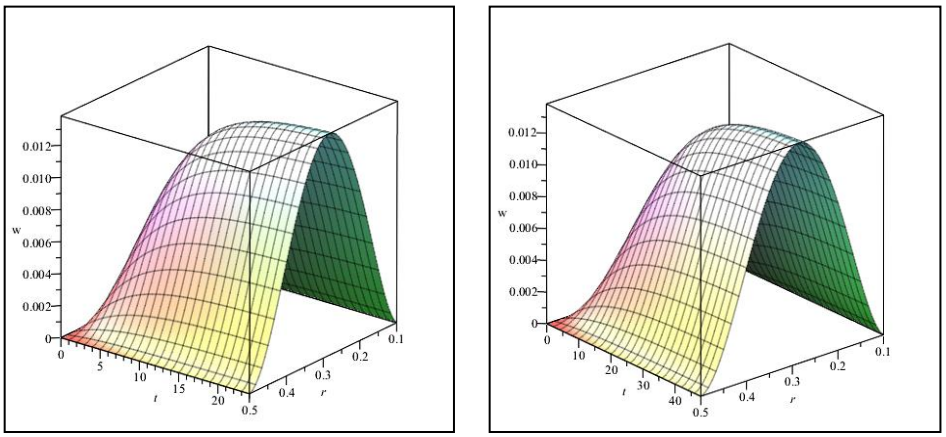


Figure 9. Deflection changes versus r and time for (**a**) $g = 5$ and (**b**) $g = 10$.

7. Conclusions

The present study investigated the viscoelastic analysis of nonlinear elastic (hyperelastic) materials. The governing partial differential equations and mathematical definitions of boundary conditions were derived based on a new method and were solved by the semi-analytical method based on polynomials (SAPM). The viscoelastic property of the structural material is assumed by Kelvin–Voigt modeling. In general, the significant results obtained from the research can be categorized as follows:

1. The new theory of hyperelastic structures can be used with appropriate confidence for viscoelastic properties.
2. Structures made of nonlinear elastic material are sensitive to changes in applied transverse loads, and the changes are entirely nonlinear, even with the low-load application.
3. For low loads, it has a significant impact on the deformation by the boundary conditions. However, as the load increases, these effects decrease.
4. As the viscosity increases, the duration of the final deformation increases, which has a direct relationship with the viscosity of the material.

Author Contributions: Conceptualization, S.D. and B.A.; methodology, S.D.; software, S.D.; validation, S.D.; formal analysis, S.D.; investigation, S.D.; resources, B.A.; data curation, S.D.; writing—original draft preparation, B.A.; writing—review and editing, B.A. and Ö.C; visualization, B.A.; supervision, Ö.C.; project administration, Ö.C.; and funding acquisition, Ö.C. All authors have read and agreed to the published version of the manuscript.

Funding: This research received no external funding.

Institutional Review Board Statement: Not applicable.

Informed Consent Statement: Not applicable.

Data Availability Statement: There is no data for sharing, and all data are available within the paper.

Conflicts of Interest: The authors declare no conflict of interest.

References

1. Boyce, M.C.; Arruda, E.M. Constitutive models of rubber elasticity: A review. *Rubber Chem. Technol.* **2000**, *73*, 504–523. [CrossRef]
2. Gent, A.N. A new constitutive relation for rubber. *Rubber Chem. Technol.* **1996**, *69*, 59–61. [CrossRef]
3. Anssari-Benam, A.; Bucchi, A. A generalised neo-Hookean strain energy function for application to the finite deformation of elastomers. *Int. J. Non-Linear Mech.* **2021**, *128*, 103626. [CrossRef]
4. Yeoh, O.H. Characterization of Elastic Properties of Carbon-Black-Filled Rubber Vulcanizates. *Rubber Chem. Technol.* **1990**, *63*, 792–805. [CrossRef]
5. Erchiqui, F.; Gakwaya, A.; Rachik, M. Dynamic finite element analysis of nonlinear isotropic hyperelastic and viscoelastic materials for thermoforming applications. *Polym. Eng. Sci.* **2005**, *45*, 125–134. [CrossRef]

6. Kocaturk, T.; Akbas, S.D. Geometrically nonlinear static analysis of a simply supported beam made of hyperelastic material. *Struct. Eng. Mech.* **2010**, *35*, 677–697. [CrossRef]
7. Li, Y.L.; Oh, I.; Chen, J.H.; Zhang, H.H.; Hu, Y.H. Nonlinear dynamic analysis and active control of visco-hyperelastic dielectric elastomer membrane. *Int. J. Solids Struct.* **2018**, *152*, 28–38. [CrossRef]
8. Alibakhshi, A.; Dastjerdi, S.; Akgoz, B.; Civalek, O. Parametric vibration of a dielectric elastomer microbeam resonator based on a hyperelastic cosserat continuum model. *Compos. Struct.* **2022**, *287*, 115386. [CrossRef]
9. Almasi, A.; Baghani, M.; Moallemi, A. Thermomechanical analysis of hyperelastic thick-walled cylindrical pressure vessels, analytical solutions and FEM. *Int. J. Mech. Sci.* **2017**, *130*, 426–436. [CrossRef]
10. Asgari, M.; Hashemi, S.S. Dynamic visco-hyperelastic behavior of elastomeric hollow cylinder by developing a constitutive equation. *Struct. Eng. Mech.* **2016**, *59*, 601–619. [CrossRef]
11. Pascon, J.P. Finite element analysis of functionally graded hyperelastic beams under plane stress. *Eng. Comput.* **2020**, *36*, 1265–1288. [CrossRef]
12. Pascon, J.P. Large deformation analysis of functionally graded visco-hyperelastic materials. *Comput. Struct.* **2018**, *206*, 90–108. [CrossRef]
13. Gharooni, H.; Ghannad, M. Nonlinear analysis of radially functionally graded hyperelastic cylindrical shells with axially-varying thickness and non-uniform pressure loads based on perturbation theory. *J. Comput. Appl. Mech.* **2019**, *50*, 324–340.
14. Hosseini, S.; Rahimi, G. Nonlinear Bending Analysis of Hyperelastic Plates Using FSDT and Meshless Collocation Method Based on Radial Basis Function. *Int J Appl Mech* **2021**, *13*, 2150007. [CrossRef]
15. Xu, Q.P.; Liu, J.Y.; Qu, L.Z. A Higher-Order Plate Element Formulation for Dynamic Analysis of Hyperelastic Silicone Plate. *J. Mech.* **2019**, *35*, 795–808. [CrossRef]
16. Dadgar-Rad, F.; Firouzi, N. Large deformation analysis of two-dimensional visco-hyperelastic beams and frames. *Arch. Appl. Mech.* **2021**, *91*, 4279–4301. [CrossRef]
17. Ansari, R.; Hassani, R.; Oskouie, M.F.; Rouhi, H. Nonlinear bending analysis of hyperelastic Mindlin plates: A numerical approach. *Acta Mech.* **2021**, *232*, 741–760. [CrossRef]
18. Tashiro, K.; Shobayashi, Y.; Ota, I.; Hotta, A. Finite element analysis of blood clots based on the nonlinear visco-hyperelastic model. *Biophys. J.* **2021**, *120*, 4547–4556. [CrossRef] [PubMed]
19. Shariyat, M.; Abedi, S. An accurate hyperelasticity-based plate theory and nonlinear energy-based micromechanics for impact and shock analyses of compliant particle-reinforced FG hyperelastic plates. *Zamm-Z. Angew. Math. Mech.* **2022**, *102*, e202100099. [CrossRef]
20. Karimi, S.; Ahmadi, H.; Foroutan, K. Nonlinear vibration and resonance analysis of a rectangular hyperelastic membrane resting on a Winkler-Pasternak elastic medium under hydrostatic pressure. *J. Vib. Control* **2022**. [CrossRef]
21. Alibakhshi, A.; Heidari, H. Nonlinear dynamics of dielectric elastomer balloons based on the Gent-Gent hyperelastic model. *Eur. J. Mech. A-Solid* **2020**, *82*, 103986. [CrossRef]
22. Alibakhshi, A.; Rahmanian, S.; Dastjerdi, S.; Malikan, M.; Karami, B.; Akgoz, B.; Civalek, O. Hyperelastic Microcantilever AFM: Efficient Detection Mechanism Based on Principal Parametric Resonance. *Nanomaterials* **2022**, *12*, 2598. [CrossRef] [PubMed]
23. Falope, F.O.; Lanzoni, L.; Tarantino, A.M. FE Analyses of Hyperelastic Solids under Large Bending: The Role of the Searle Parameter and Eulerian Slenderness. *Materials* **2020**, *13*, 1597. [CrossRef] [PubMed]
24. Hosseini, S.; Rahimi, G.; Shahgholian-Ghahfarokhi, D. A meshless collocation method on nonlinear analysis of functionally graded hyperelastic plates using radial basis function. *Zamm-Z. Angew. Math. Mech.* **2022**, *102*, e202100216. [CrossRef]
25. Coda, H.B.; Bernardo, C.C.L.G.; Paccola, R.R. A FEM formulation for the analysis of laminated and functionally graded hyperelastic beams with continuous transverse shear stresses. *Compos. Struct.* **2022**, *292*, 115606. [CrossRef]
26. Dastjerdi, S.; Alibakhshi, A.; Akgoz, B.; Civalek, O. A Novel Nonlinear Elasticity Approach for Analysis of Nonlinear and Hyperelastic Structures. *Eng. Anal. Bound. Elem.* **2022**, *143*, 219–236. [CrossRef]
27. Zhao, Z.T.; Niu, D.T.; Zhang, H.W.; Yuan, X.G. Nonlinear dynamics of loaded visco-hyperelastic spherical shells. *Nonlinear Dyn.* **2020**, *101*, 911–933. [CrossRef]
28. Zhao, Z.T.; Yuan, X.G.; Zhang, W.Z.; Niu, D.T.; Zhang, H.W. Dynamical modeling and analysis of hyperelastic spherical shells under dynamic loads and structural damping. *Appl. Math. Model.* **2021**, *95*, 468–483. [CrossRef]
29. Bacciocchi, M.; Tarantino, A.M. Bending of hyperelastic beams made of transversely isotropic material in finite elasticity. *Appl. Math. Model.* **2021**, *100*, 55–76. [CrossRef]
30. Khaniki, H.B.; Ghayesh, M.H.; Chin, R.; Amabili, M. A review on the nonlinear dynamics of hyperelastic structures. *Nonlinear Dyn.* **2022**, *110*, 963–994. [CrossRef]
31. Zenkour, A.M. Nonlocal thermal vibrations of embedded nanoplates in a viscoelastic medium. *Struct. Eng. Mech.* **2022**, *82*, 701–711.
32. Yuan, Y.; Niu, Z.Q.; Smitt, J. Magneto-hygro-thermal vibration analysis of the viscoelastic nanobeams reinforcedwith carbon nanotubes resting on Kerr's elastic foundation based on NSGT. *Adv. Compos. Mater.* **2022**. [CrossRef]
33. Soleimani-Javid, Z.; Arshid, E.; Amir, S.; Bodaghi, M. On the higher-order thermal vibrations of FG saturated porous cylindrical micro-shells integrated with nanocomposite skins in viscoelastic medium. *Def. Technol.* **2022**, *18*, 1416–1434. [CrossRef]

34. Moayeri, M.; Darabi, B.; Sianaki, A.H.; Adamian, A. Third order nonlinear vibration of viscoelastic circular microplate based on softening and hardening nonlinear viscoelastic foundation under thermal loading. *Eur. J. Mech. A-Solid* **2022**, *95*, 104644. [CrossRef]
35. Li, Y.; Liu, B. Thermal buckling and free vibration of viscoelastic functionally graded sandwich shells with tunable auxetic honeycomb core. *Appl. Math. Model.* **2022**, *108*, 685–700. [CrossRef]
36. Dang, R.Q.; Yang, A.M.; Chen, Y.M.; Wei, Y.Q.; Yu, C.X. Vibration analysis of variable fractional viscoelastic plate based on shifted Chebyshev wavelets algorithm. *Comput. Math. Appl.* **2022**, *119*, 149–158. [CrossRef]
37. Alizadeh, A.; Shishehsaz, M.; Shahrooi, S.; Reza, A. Free vibration characteristics of viscoelastic nano-disks based on modified couple stress theory. *J. Strain Anal. Eng.* **2022**. [CrossRef]
38. Ghobadi, E.; Shutov, A.; Steeb, H. Parameter Identification and Validation of Shape-Memory Polymers within the Framework of Finite Strain Viscoelasticity. *Materials* **2021**, *14*, 2049. [CrossRef]
39. Dacol, V.; Caetano, E.; Correia, J.R. A New Viscoelasticity Dynamic Fitting Method Applied for Polymeric and Polymer-Based Composite Materials. *Materials* **2020**, *13*, 5213. [CrossRef]
40. Chang, J.J.; Li, Y.Y.; Zeng, X.F.; Zhong, H.Y.; Wan, T.L.; Lu, C. Study on the Viscoelasticity Measurement of Materials Based on Surface Reflected Waves. *Materials* **2019**, *12*, 1875. [CrossRef] [PubMed]
41. Wang, D.Z.; de Boer, G.; Ghanbarzadeh, A. A Numerical Model for Investigating the Effect of Viscoelasticity on the Partial Slip Solution. *Materials* **2022**, *15*, 5182. [CrossRef] [PubMed]
42. Itou, H.; Kovtunenko, V.A.; Rajagopal, K.R. The Boussinesq flat-punch indentation problem within the context of linearized viscoelasticity. *Int. J. Eng. Sci.* **2020**, *151*, 103272. [CrossRef]
43. Dastjerdi, S.; Akgoz, B.; Civalek, O. On the effect of viscoelasticity on behavior of gyroscopes. *Int. J. Eng. Sci.* **2020**, *149*, 103236. [CrossRef]
44. Dastjerdi, S.; Akgoz, B.; Civalek, O. On the shell model for human eye in Glaucoma disease. *Int. J. Eng. Sci.* **2021**, *158*, 103414. [CrossRef]
45. Dastjerdi, S.; Malikan, M.; Akgoz, B.; Civalek, O.; Wiczenbach, T.; Eremeyev, V.A. On the deformation and frequency analyses of SARS-CoV-2 at nanoscale. *Int. J. Eng. Sci.* **2022**, *170*, 103604. [CrossRef]
46. Li, C.; Zhu, C.; Sui, S.; Yan, J. A Perturbation Approach for Lateral Excited Vibrations of a Beam-like Viscoelastic Microstructure Using the Nonlocal Theory. *Appl. Sci.* **2022**, *12*, 40. [CrossRef]
47. Hu, W.; Xu, M.; Song, J.; Gao, Q.; Deng, Z. Coupling dynamic behaviors of flexible stretching hub-beam system. *Mech. Syst. Signal Process.* **2021**, *151*, 107389. [CrossRef]
48. Yan, J.W.; Lai, S.K.; He, L.H. Nonlinear dynamic behavior of single-layer graphene under uniformly distributed loads. *Compos. B Eng.* **2019**, *165*, 473–490. [CrossRef]
49. Pascon, J.P.; Coda, H.B. Finite deformation analysis of visco-hyperelastic materials via solid tetrahedral finite elements. *Finite Elem. Anal. Des.* **2017**, *133*, 25–41. [CrossRef]
50. López-Campos, J.A.; Segade, A.; Fernández, J.R.; Casarejos, E.; Vilán, J.A. Behavior characterization of visco-hyperelastic models for rubber-like materials using genetic algorithms. *Appl. Math. Model.* **2019**, *66*, 241–255. [CrossRef]
51. Yarali, E.; Baniasadi, M.; Bodaghi, M.; Bodaghi, M. 3D constitutive modeling of electro-magneto-viscohyperelastic elastomers: A semi-analytical solution for cylinders under large torsion–extension deformation. *Smart Mater. Struct.* **2020**, *29*, 085031. [CrossRef]
52. Dastjerdi, S.; Tadi Beni, Y.; Malikan, M. A comprehensive study on nonlinear hygro-thermo-mechanical analysis of thick functionally graded porous rotating disk based on two quasi-three-dimensional theories. *Mech Based Des Struct* **2022**, *50*, 3596–3625. [CrossRef]
53. Zhang, D.G.; Zhou, H.M. Nonlinear bending analysis of FGM circular plates based on physical neutral surface and higher-order shear deformation theory. *Aerosp. Sci. Technol.* **2015**, *41*, 90–98. [CrossRef]